RSC Advances

PAPER

View Article Online
View Journal | View Issue

Cite this: *RSC Adv.*, 2020, **10**, 5845

Effects of WO_3 and SiO_2 doping on CeO_2–TiO_2 catalysts for selective catalytic reduction of NO with ammonia

Rongrong Fan,[ab] Zhaoqiang Li,*[ab] Yan Wang,[ab] Cheng Zhang,[ab] Yu Wang,[ab] Zhiyong Ding,[ab] Xin Guo[ab] and Rong Wang[ab]

Received 3rd January 2020
Accepted 27th January 2020

DOI: 10.1039/d0ra00053a

rsc.li/rsc-advances

A series of CeO_2–WO_3/SiO_2–TiO_2 (CeW_xTiSi_y) catalysts with different loading amounts of WO_3 were synthesized by wet co-impregnation of ammonium metatungstate and cerium nitrate on a SiO_2–TiO_2 support, and were employed for the selective catalytic reduction (SCR) of NO by NH_3. The catalytic activity of the CeO_2/SiO_2–TiO_2 (CeSiTi) catalyst was enhanced by the addition of WO_3, and the W-containing catalysts showed higher hydrothermal stability especially between 550 and 600 °C. The introduction of WO_3 to the CeSiTi catalyst could produce more chemisorbed oxygen species, reducible subsurface oxygen species, acid sites and ad-NO_x species. Moreover, the modification of CeO_2–WO_3/TiO_2 (CeWTi) by SiO_2 could enhance the specific surface area, especially the aged specific surface area, thus improving the hydrothermal stability of the catalyst.

1. Introduction

Nitrogen oxides (NO_x) are one of the major sources of air pollution, and have caused a series of environmental problems such as acid rain, photochemical smog, and the green-house effect.[1–3] The emission of NO_x remains a major problem for diesel vehicles. In recent years, great efforts have been applied to the development and application of available technologies for controlling NO_x emissions. Among these technologies, selective catalytic reduction (SCR) of NO_x using reductants such as NH_3 or hydrocarbons (HC) is one of the most promising technologies to reduce NO_x. The issue of catalyst deactivation by HC poisoning needs to be resolved for the commercial application of HC–SCR.[4] Currently, the SCR of NO_x with NH_3 (NH_3–SCR) is the favored method of denoxification ($deNO_x$), which has also been widely employed commercially for diesel vehicles to meet the ever tightening emission standards.[5–8]

Many types of catalysts, including oxides and zeolites based on transition metals have been investigated for the NH_3–SCR reaction.[9] However, these catalysts have intrinsic flaws when it comes to practical applications. Transition-metal (in particular Fe and Cu) ion-exchanged zeolite catalysts have poor water and sulfur resistances.[10] V_2O_5-based oxide catalysts have been used commercially for SCR due to its high catalytic activity and resistance to SO_2 poisoning, whereas the toxicity of vanadium, the easy sublimation of V_2O_5 and narrow catalytic temperature window (300–400 °C) of this catalyst limit their wide application.[11,12] Therefore, great efforts have been made to develop environmental friendly SCR catalysts to replace V_2O_5-based catalysts. Studies in recent years revealed that the presence of rare-earth components can effectively regulate the surface acidity and alkalinity, modify the structure of catalytic active centers, improve the oxygen storage/release capacities, and enhance the structural stability and active species dispersion of catalysts.[13,14]

As an important component of rare-earth catalytic materials, CeO_2 is a potential substitute for V_2O_5 due to its high oxygen storage capacity and redox ability when Ce species shift between Ce^{4+} and Ce^{3+}.[15,16] Various studies have been conducted to develop SCR catalysts using CeO_2, and several catalyst systems have been developed, including CeO_2/TiO_2,[17] CeO_2/TiO_2–SiO_2,[18] CeO_2/WO_3,[19] CeO_2/ZrO_2,[20] *etc.* The selection of supports is important for the performance of the composite catalysts in environmental catalytic reactions, because the structural properties of supports can affect the dispersion of active sites and the contact between reactants. Various types of supports, such as Al_2O_3,[21] medicinal stone,[22] Ti-pillared clays,[23] TiO_2,[24] have been used in environmental catalytic reactions of photocatalysis, catalytic oxidative desulfurization and organic pollutants degradation. Among them, TiO_2 is a favorable candidate as the support for SCR catalysts due to its good SO_2 durability and stability,[25] hence CeO_2/TiO_2 catalyst exhibits higher SCR catalytic activity. Moreover, WO_3 is widely used as a promotional additive to enhance the catalytic activity of V_2O_5/TiO_2 catalyst. It was reported that introduction of WO_3 to V_2O_5/TiO_2 increased the amount and the strength of Brönsted acid

[a]State Key Laboratory of Baiyunobo Rare Earth Resource Researches and Comprehensive Utilization, Baotou Research Institute of Rare Earths, Baotou 014030, China. E-mail: li_brire@163.com

[b]National Engineering Research Center of Rare Earth Metallurgy and Functional Materials, Baotou 014030, China

sites on the catalyst surface.[26] CeO_2/WO_3 catalyst also exhibits very high efficiency for the reduction of NO_x.[27] Shan *et al.* examined the promotional effects of a tungsten-doped CeO_2/TiO_2 catalyst and the excellent catalytic performance of the CeO_2–WO_3/TiO_2 catalyst was associated with the highly dispersed CeO_2 and primitive WO_3 species on TiO_2.[28] Furthermore, SiO_2 is widely used as catalyst supports due to their high mechanical strength and excellent thermal stability.[29,30] TiO_2 is usually mixed with SiO_2 as the support to enhance the thermal stability and prevent the deactivating during exposure to SO_2.[31] However, seldom studies focus on CeO_2–WO_3/TiO_2–SiO_2 catalyst.

In this paper, a series of CeO_2–WO_3/TiO_2–SiO_2 catalysts were prepared by impregnation method and their SCR performance were evaluated in a simulated diesel engine exhaust. According to the characterization, the essence of the activity enhancement arising from the WO_3 and SiO_2 introduction and the active species for the reaction were proposed and elucidated in detail.

2. Experimental

2.1 Catalyst preparation

A series of CeO_2–WO_3/TiO_2–SiO_2 catalysts with different WO_3 loading amount (denoted as CeW_xSi_yTi; x represents the weight percent of WO_3, x = 0–8%; y represents the weight percent of SiO_2, y = 0 or 5%) were prepared by the co-impregnation method. Cerium nitrate ($(CeNO_3)_3\cdot 6H_2O$), ammonium metatungstate ($(NH_4)_6W_7O_{24}\cdot 6H_2O$), and TiO_2–SiO_2/TiO_2 support were used for the experiment. All the chemicals with purity ≥99.7% are from Sinopharm Chemical Reagent Co., Ltd, China. Firstly, cerium nitrate and ammonium metatungstate were dissolved in deionized water. TiO_2–SiO_2 or TiO_2 powder was added to the above solution and stirred for 1 h. Secondly, the mixture exposed to ultrasonic for 2 h and then aged for 12 h. At last, the mixture was dried at 110 °C for 2 h and calcined at 550 °C for 3 h in static air. CeO_2 contents in all the catalysts were 20 wt%.

The fresh catalyst was thermally aged in 10% H_2O in air at 600 °C for 50 h and labeled as aged-600 °C 50 h.

2.2 Catalytic activity measurement

The activity test of 0.06 g catalysts was carried out in a fixed-bed quartz reactor (inner diameter = 6 mm). The gas mixture simulates a real diesel exhaust, which contains 200 ppm NO, 200 ppm NH_3, 200 ppm CO, 50 ppm C_3H_6, 12 vol% O_2, 5 vol% H_2O, 4.5 vol% CO_2, and N_2 as balance gas. The total flow rate was 300 mL min^{-1}, corresponding to GHSV of 300 000 h^{-1}. The effluent gas, including NO, NO_2, and O_2 was continuously analyzed by an online flue gas analyzer. The results for the steady-state activity were collected after 20 min at each temperature. The NO_x conversion was calculated as follows, whereas NO_x = NO + NO_2.

$$NO_x \text{ conversion} = \frac{c[NO_x]\text{inlet} - c[NO_x]\text{outlet}}{c[NO_x]\text{inlet}} \times 100\%$$

2.3 Catalysts characterization

The BET surface area was measured at −196 °C on an ASAP 2050 physical adsorption instrument (Micromeritics Corp., Norcross, GA, USA) by using the nitrogen adsorption method. The samples were pretreated in a vacuum at 300 °C for 4 h before experiments. The surface area was determined by BET method in 0–0.3 partial pressure range.

X-ray diffraction (XRD) measurement was performed on an X′pert Pro diffractometer (Panalytical Corp., The Netherlands) operating at 40 mA and 40 kV with Cu Kα radiation. The 2θ data from 10 to 90° were collected with the step size of 0.03°.

Microstructures of the catalyst samples were observed with a FEI Tecnai G2 F20 electron microscope.

X-ray photoelectron spectra (XPS) were obtained with a Thermo ESCALAB 250Xi spectrometer (ThermoFisher Scientific, Waltham, MA, USA) using Al Kα radiation (1486.6 eV). Binding energies of Ce 3d and O 1s were calibrated using C 1s peak (B.E. = 284.6 eV) as standard. The composition on catalyst surface according to atomic ratios was calculated, and Shirley background and Gaussian–Lorentzian was used for peak analysis.

H_2 temperature programmed reduction (H_2-TPR) was carried out on a Quantachrome: Chem BET chemisorption analyzer (Micromeritics, Norcross, GA, USA). Before the experiment, 50 mg of the sample was heated from room temperature to 800 °C at a rate of 10 °C min^{-1}. A mixture gas flow of 5 vol% H_2/Ar was used as reductant at a flow rate of 60 mL min^{-1}. Before detection by the TCD, the gas was purified by a trap containing CaO + NaOH materials in order to remove the H_2O and CO_2.

The temperature-programmed desorption (TPD) of NH_3 or NO_x was conducted on a Quantachrome: Chem BET chemisorption analyzer supplied by the Micromeritics Company. 50 mg of the sample was pretreated at 300 °C (10 °C min^{-1}) in He flow at 60 mL min^{-1} for 2 h, then cooled down to 40 °C and purged with 5 vol% NH_3/He (500 ppm NO + 3% O_2) until adsorption saturation, followed by flushing with 20 mL min^{-1} He at the same temperature to remove physical absorption species. The desorption was then performed in the range of 40–800 °C at a speed of 10 °C min^{-1}.

3. Results and discussion

3.1 SCR catalytic activity

The effect of WO_3 and SiO_2 addition on the deNO_x performance of CeTi catalyst is illustrated in Fig. 1. As shown in Fig. 1a, CeTi and CeW_4Ti showed higher NO_x conversion than CeSiTi and CeW_4SiTi, respectively, indicating that the catalytic activity was even suppressed by SiO_2. While the negative effect on CeW_4SiTi was less obvious for catalysts with WO_3 loaded, suggesting that WO_3 had a promotional impact on activity, which can also be seen from CeTi and CeWTi catalyst. NO_x conversion over CeW_4Ti was higher than CeTi at 150–550 °C. Furthermore, CeW_xSiTi catalysts with different WO_3 loadings were prepared to investigate the effect of WO_3. It was clear that the addition of WO_3 to CeSiTi could significantly enhance the catalytic activities and broaden reactivity window. CeSiTi catalyst exhibited

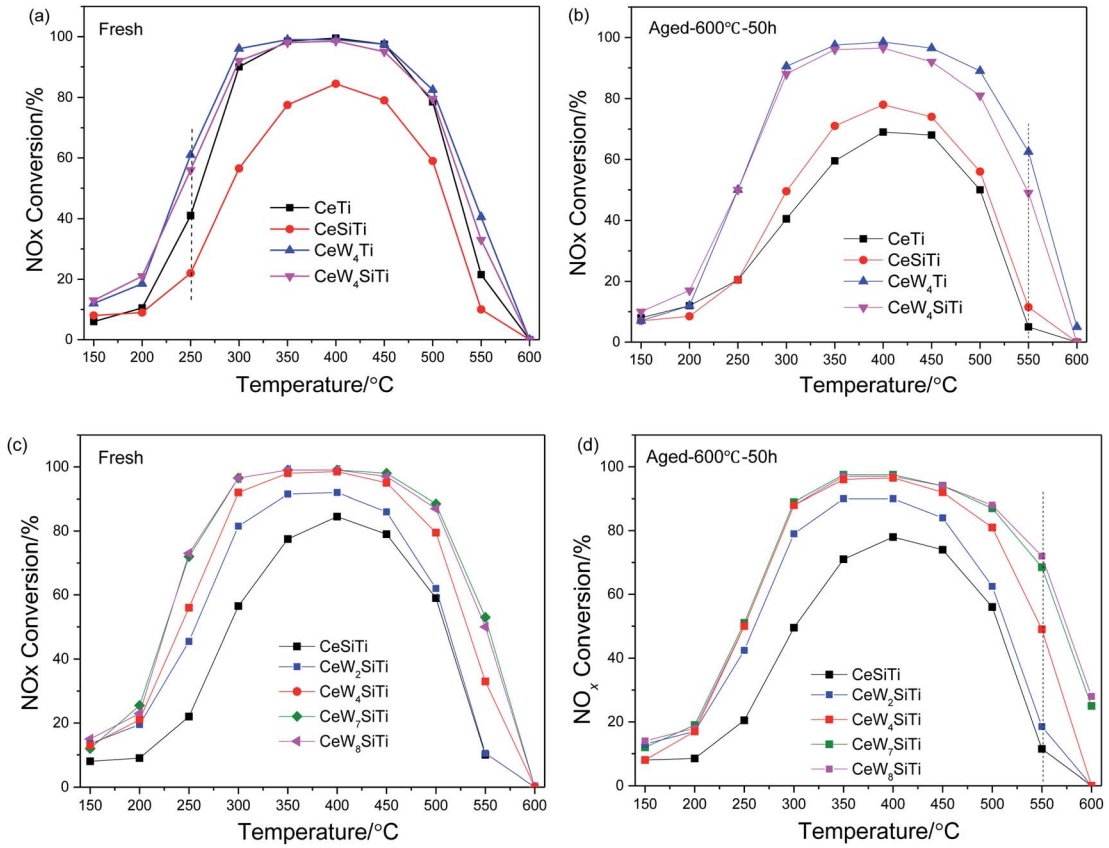

Fig. 1 Effect of WO_3 and SiO_2 over CeW_xTiSi_y catalysts on deNO_x performance. (a) and (c) Fresh samples; (b) and (d) thermally aged samples.

relatively low activities in the whole temperature range, with maximum NO_x conversion of 84% at 400 °C. After the addition of WO_3, NO_x conversion of CeW_2SiTi was ~20% greater at 250–350 °C and ~10% at 250 or 400 °C than CeSiTi, and the maximum NO_x conversion reached to 92%. With the increasing of WO_3 loading from 2% to 7%, NO_x conversion especially at 250 °C was greatly improved from 22% to 72%. For CeW_7SiTi catalyst, nearly 100% NO_x conversion was obtained in the temperature range of 300–450 °C. Further increasing the WO_3 loading to 8%, CeW_8SiTi showed nearly the same catalytic activity as CeW_7SiTi. This suggested that the WO_3 addition amount is close to its distributed capacity.[32]

SCR performance of the catalysts after hydrothermal aging treatment is shown in Fig. 1b and d. Compared with the fresh sample, activity of aged CeTi dropped dramatically in a wide temperature range of 250–550 °C. The maximum decrease of NO_x conversion appearing at 300 °C was up to 50%, indicating that hydrothermal aging had a severe impact on CeTi catalyst. In contrast, NO_x conversion of CeSiTi decreased slightly with only 7% drop at 300 °C, demonstrating that SiO_2 could greatly enhanced thermal stability of catalysts. For catalysts with WO_3 doped (CeW_4Ti and CeW_xSiTi), catalytic activities were remained after hydrothermally treated. Remarkably, compared with the fresh samples, NO_x conversions of these catalysts at temperature 550–600 °C were even higher. For example, NO_x conversion of aged CeW_4Ti and CeW_xSiTi at 550 °C were 22% and 16% higher than that of their fresh samples, respectively. Therefore, WO_3 and SiO_2 were synergistically beneficial for hydrothermal stability of the catalysts.

To evaluate the stability of the catalyst, CeW_7SiTi was chosen to carry out the reuse cycle experiment, as described on sub-Section 2.2. After one test cycle finished, the sample was cooled down to room temperature first, then heated to 600 °C for another cycle. Catalytic activities in each cycle were exhibited in Fig. 2. It can be seen that there was no obvious reduction in the catalytic activity after 7 reuse cycles, indicating perfect reusability and good stability of the catalyst.

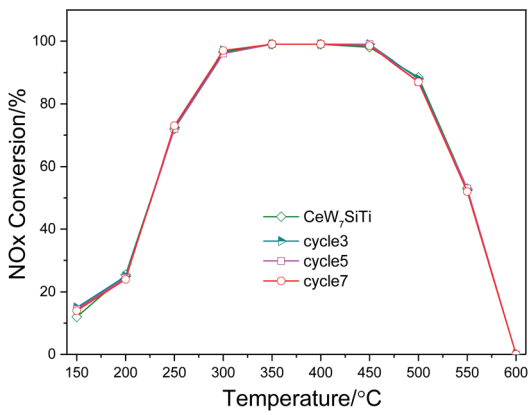

Fig. 2 Reuse cycle experiment of CeW_7SiTi catalyst.

3.2 XRD and BET results

The XRD patterns of CeW_xSi_yTi catalysts are shown in Fig. 3. Only diffraction peaks attributed to cubic CeO_2 crystallites (ICDD PDF#34-0394) and anatase phase (ICDD PDF# 21-1272) of TiO_2 were detected, no WO_3 or SiO_2 phase was observed,[16] which suggested that W and Si species probably exist in an amorphous phase or as highly dispersed species.[33] The intensities of CeO_2 peak slowly increased with the WO_3 content increasing, indicating that CeO_2 crystallites grown slowly, which may be due to the blocking effect of the CeO_2 by the impregnated tungsten oxide.[34] Accordingly, the average crystallite size calculated using the Scherrer equation is shown in Table 1. The crystallite size increased from 15.4 nm to 17.0 nm with WO_3 loadings of CeW_xSiTi increasing from 0% to 8%. Moreover, as presented in Table 1, the lattice parameter corresponding to the ceria phase was also calculated *via* Bragg's Law.[35] The lattice constant and *d*-spacing of CeO_2 increased a little by impregnating tungsten oxide. For CeW_xSiTi, *d*-spacing expanded from 0.268 nm to 0.272 nm, and the lattice constant increased from 0.533 nm to 0.535 nm. Likewise for CeW_xTi catalysts, from CeTi to CeW_4Ti, crystallite size elevated from 16.3 nm to 17.3 nm, *d*-spacing from 0.267 nm to 0.271 nm, and lattice constant from 0.532 nm to 0.534 nm. Generally, the lattice constant of ceria is mainly associated with the ratio of Ce^{3+} (0.110 nm)/Ce^{4+} (0.087 nm).[34] Therefore, the increasing lattice constant may be result from more Ce^{3+} species brought by WO_3 incorporation, as discussed in the following XPS results.

The HR-TEM micrographs of different catalysts are exhibited in Fig. 4. Particle size of CeTi and CeW_4Ti catalysts were about 10–20 nm. For CeTi, lattice fringes of 0.272 nm and 0.351 nm matched CeO_2 (200) and anatase (101) phase, respectively.[2] After addition of WO_3, lattice fringe of CeO_2 (200) increase to 0.278 nm, which was consistent with the XRD results.

The BET surface areas of CeW_xTiSi_y catalysts as well as total pore volumes and average pore diameters are presented in Table 2. It is clear that with WO_3 content increasing, a slight decrease in BET surface area is observed. This may be due to the growing cluster of CeO_2 crystallites causing the agglomeration of the catalyst surface according to the XRD results.[36]

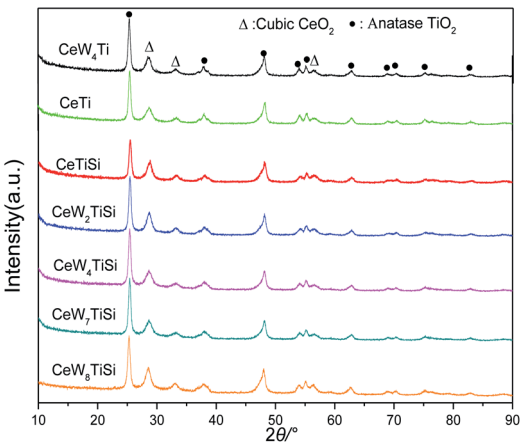

Fig. 3 XRD patterns of CeW_xSi_yTi catalysts with different WO_3 loadings.

Table 1 Crystallite size and lattice parameter of the catalysts

Catalysts	Crystallite size of CeO_2 (nm)	*d*-spacing (nm)	Lattice constant of CeO_2 (nm)
CeTi	16.3	0.267	0.532
CeW_4Ti	17.3	0.271	0.534
CeSiTi	15.4	0.268	0.533
CeW_2SiTi	15.9	0.268	0.534
CeW_4SiTi	16.5	0.268	0.534
CeW_7SiTi	16.5	0.268	0.534
CeW_8SiTi	17.0	0.272	0.535

Compared with that of their fresh counterpart, the total pore volumes and average pore diameters of aged CeW_xTiSi_y catalysts increased, while BET surface area decreased. Notably for CeTi, BET surface area drastically dropped from 67 to 42 $m^2\ g^{-1}$ (a 37.3% decrease). Whereas the surface area loss of CeW_4Ti and CeW_xTiSi were much lower (7.8–13.6%), indicating hydrothermal stability was improved by addition of WO_3 and SiO_2. Remarkably, the BET surface area of aged CeSiTi (80 $m^2\ g^{-1}$) is almost the same as the fresh sample (81 $m^2\ g^{-1}$), showing excellent hydrothermal stability. All these indicated that the addition of active component WO_3 and SiO_2 could coordinatively preserve the BET surface area of hydrothermally aged catalysts, thus enhance hydrothermal stability of the catalysts, which were in good accordance with results demonstrated in Fig. 1.

3.3 XPS results

To understand the chemical states of elements over the surface of CeW_xTiSi_y catalysts, XPS spectra of Ce and O are presented in Fig. 5. XPS spectra of Ce 3d are shown as Fig. 5a. The sub-bands labeled u1 and v1 represent the $3d^{10}4f^1$ initial electronic state, corresponding to Ce^{3+}, whereas the peaks labeled u, u2, u3, v, v2, and v3 represent the $3d^{10}4f^0$ state of Ce^{4+} ions. $Ce^{3+}/(Ce^{3+} + Ce^{4+})$ ratio was calculated according to the area ratio of Ce peaks and displayed in Table 3. It can be seen that the addition of WO_3 to the catalyst slightly increased Ce^{3+} ratio on the surface of the catalysts. Hence, it is likely that W promote the transformation from Ce^{4+} to Ce^{3+} ions. Ce^{3+} could create more charge imbalance, vacancies, and chemisorbed oxygen on the surface, which is beneficial for SCR performance.

Fig. 5b displays the O 1s XPS spectra of different catalysts. The O 1s peaks were fitted into two sub-bands. The bands at 531.0–531.9 eV are assigned to surface-chemisorbed oxygen (denoted as O_α). And the sub-bands from 529.5 to 530.0 eV are attributable to the lattice O^{2-} oxygen (denoted as O_β). The surface-adsorbed oxygen is considered to be more reactive in oxidation reactions since its mobility is higher than that of lattice oxygen, and Wu *et al.*[37] have insisted that a high O_α ratio is beneficial for the oxidation of NO to NO_2 in the SCR reaction, resulting in an improvement to a "fast SCR" reaction. According to Table 3, $O_\alpha/(O_\alpha + O_\beta)$ ratio of CeW_xTiSi elevated from 29.2% to 48.1% as the WO_3 content increasing, thereby improving the activity of the catalysts. Similar results were obtained in CeTi & CeW_4Ti catalysts. Additionally, for CeTi and CeW_4Ti catalysts,

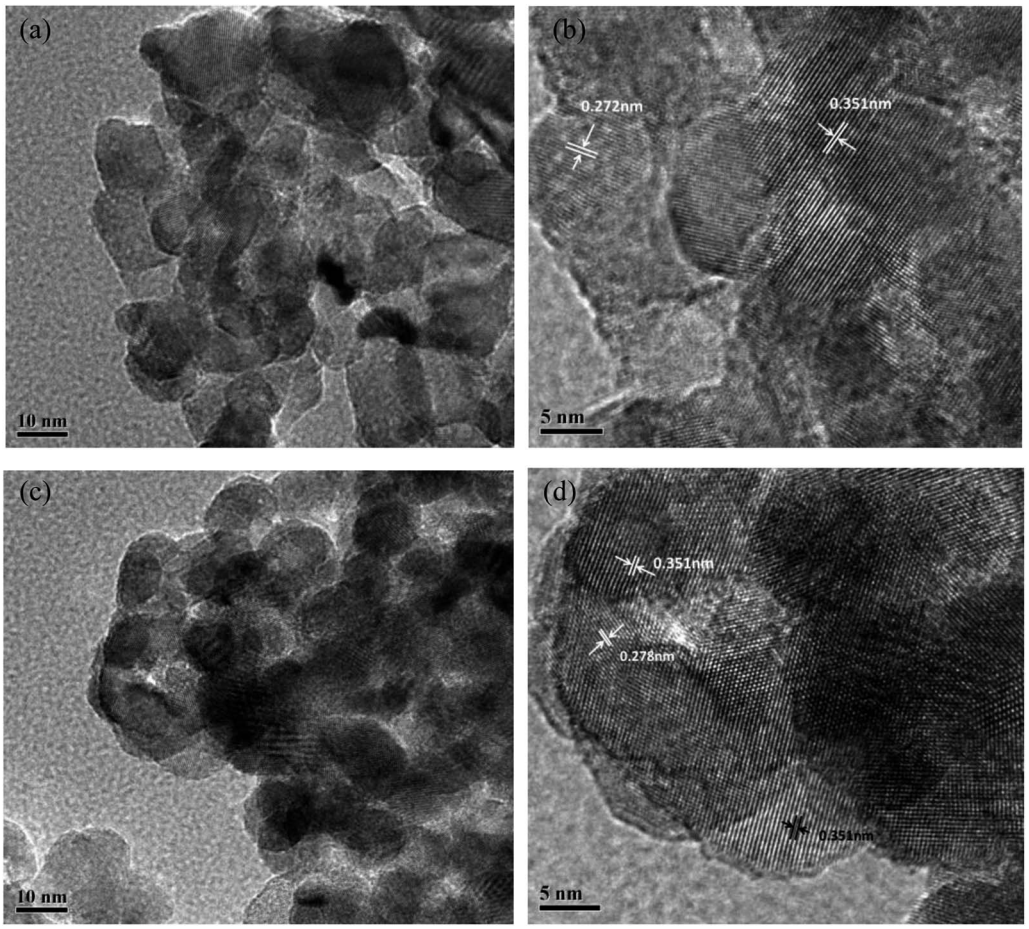

Fig. 4 TEM images of (a), (b) CeTi and (c), (d) CeW_4Ti catalysts.

SiO_2 doping increased the $O_\alpha/(O_\alpha + O_\beta)$ ratio. However, the activities of SiO_2 free catalysts were better, as shown in Fig. 1. This indicated that some synergistic effect should take place between the Ce, W species and SiO_2 support.

3.4 NO_x adsorption

To investigate the influence of WO_3 on the NO_x adsorption/desorption of the catalysts, NO_x–TPD was performed. Fig. 6 displays the TPD profiles of NO_x on the catalysts. The NO_x profiles were mainly divided into four different peaks by peak fitting according to the Gaussian deconvolution method. The first peak at 164–181 °C were associated with the desorption of physisorbed NO_x. The NO_x peak at 218–258 °C were mainly due to the decomposition of chemisorbed NO_x species. The peaks at 315–390 °C and 511–620 °C were probably related to the decomposition of bridging nitrate species and bidentate nitrate species with higher thermal stability.[38] The NO_x adsorption capacity of CeW_4SiTi and CeW_4Ti calculated in Table 4 were

Table 2 BET surface area (S_{BET}), total pore volume (V_P), average pore diameter (D_P) of CeW_xSi_yTi catalysts

	V_P ($cm^3\ g^{-1}$)		D_P (nm)		S_{BET} ($m^2\ g^{-1}$)		
	Fresh sample	Aged sample	Fresh sample	Aged sample	Fresh sample	Aged sample	ΔS_{BET}[a] (%)
CeTi	0.2685	0.2471	15.98	23.51	67	42	37.3
CeW_4Ti	0.2489	0.2632	15.19	18.35	66	57	13.6
CeSiTi	0.2487	0.2777	12.30	13.87	81	80	1.2
CeW_2SiTi	0.2302	0.2821	11.99	14.91	77	71	7.8
CeW_4SiTi	0.2326	0.2541	12.48	15.91	75	68	9.3
CeW_7SiTi	0.2328	0.2599	12.82	15.90	73	65	11.0
CeW_8SiTi	0.2331	0.2547	13.31	15.60	70	63	10.0

[a] $\Delta S_{BET} = \dfrac{S_{BET}(\text{fresh}) - S_{BET}(\text{aged})}{S_{BET}(\text{fresh})} \times 100\%$.

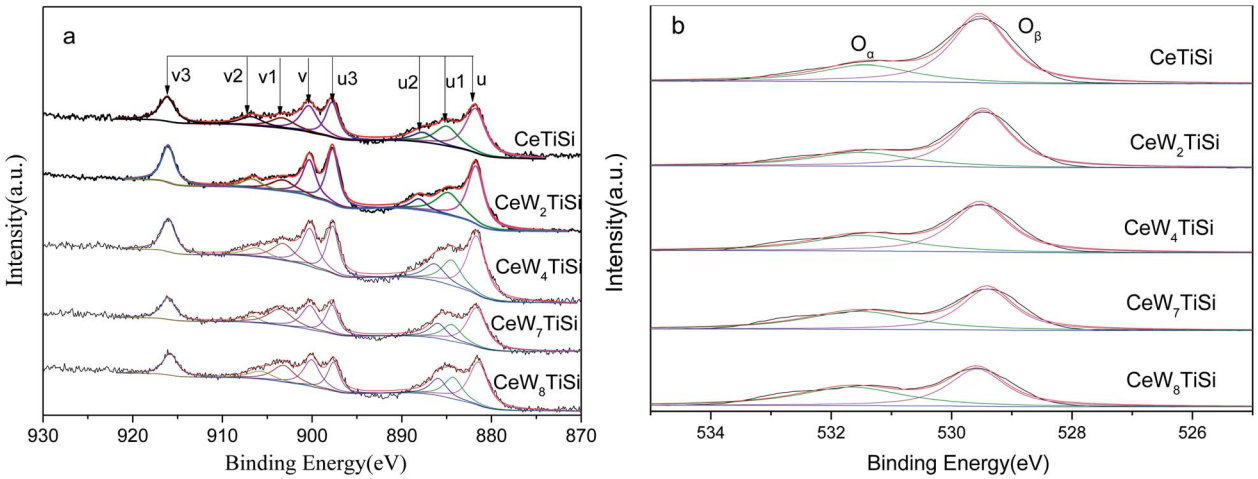

Fig. 5 XPS spectra of (a) Ce 3d and (b) O 1s for CeW_xSi_yTi catalysts.

Table 3 XPS results of CeW_xTiSi_y catalysts

Catalysts	$Ce^{3+}/(Ce^{3+} + Ce^{4+})$	$O_\alpha/(O_\alpha + O_\beta)$
CeSiTi	21.2%	29.2%
CeW_2SiTi	21.2%	30.8%
CeW_4SiTi	21.9%	36.3%
CeW_7SiTi	23.9%	47.2%
CeW_8SiTi	24.4%	48.1%
CeTi	21.1%	23.3%
CeW_4Ti	23.5%	28.7%

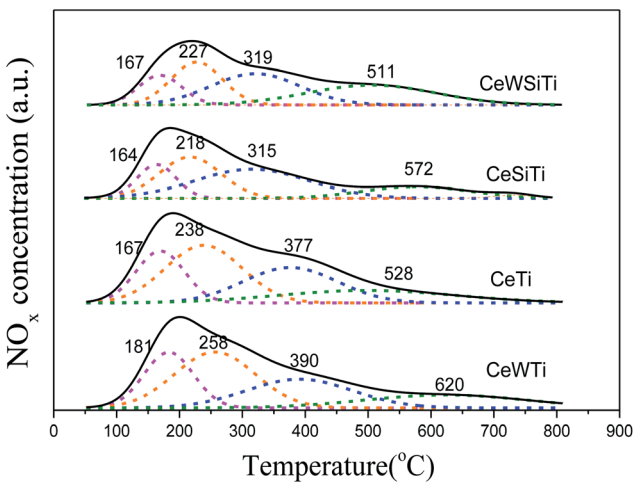

Fig. 6 NO_x–TPD profiles over the CeW_xSi_yTi catalysts.

1.29 and 2.05 mmol g^{-1}, respectively, which were higher than that of CeSiTi (1.02 mmol g^{-1}) and CeTi (1.87 mmol g^{-1}). It indicated that the addition of W increased the amount of NO_x adsorbed species. Nitrate species (ad-NO_x), formed on the catalyst surface, are known to play an important role in NO reduction. ad-NO_x species desorbed above 300 °C are presumed to participate in NO reduction.[39,40] The total areas of peaks attributed to nitrate species over WO_3-containing catalysts were larger than that over CeTi and CeSiTi catalyst, indicating the addition of W could bring more ad-NO_x species, which was beneficial for the NH_3–SCR. This elucidates the promotional effect of WO_3 on the activity of the catalysts in terms of the adsorption perspective.

3.5 Surface acidity

Surface acidity plays a critical role in SCR reaction. Surface acid sites promote ammonia adsorption on solid surfaces especially at high temperatures. The amounts and strengths of acid sites of CeW_xTiSi_y catalysts were measured by NH_3–TPD and shown in Fig. 7. All the catalysts exhibited several broad peaks in the temperature range of 100–800 °C, which were attributed to NH_3 desorbed by weak (150–350 °C), medium (350–500 °C) and strong (500–800 °C) acid sites.[37] CeTi catalyst mainly showed a single broad peak at 160 °C ascribed to NH_3 desorbed by weak acid sites. While except the first peak at around 140 °C, CeW_4Ti catalyst displayed a sharp desorption peak at 222 °C and a broad peak at 417 °C, which was ascribed to medium acid sites. Besides, its NH_3 desorption amount was 1.01 mmol g^{-1} according to Table 5, higher than 0.61 mmol g^{-1} of CeTi. CeW_xTiSi catalysts exhibited peaks at 160, 272 and 440 °C, mainly assigned to NH_3 desorption by weak and medium acid sites. With WO_3 loading amounts increasing from 0% to 8%, NH_3 desorption amount increased from 0.14 mmol g^{-1} to 2.02 mmol g^{-1}. All these results implied that the addition of WO_3 could increase amounts of acid sites of the catalysts, bringing more NH_3 adsorption sites, which plays an important role in the SCR reaction.[10]

3.6 Redox properties

H_2-TPR analysis was performed to investigate the presence of reducible species in the addition of WO_3 and SiO_2 to CeO_2/TiO_2–SiO_2. Fig. 8 illustrates the H_2-TPR profiles of CeW_xTiSi_y catalysts. All catalysts showed broad peak around 495 °C, ascribed to surface oxygen reduction of ceria.[34] CeTi catalyst presented a sharp reduction peak at 680 °C, attributing to

Table 4 NO_x adsorption capacity of catalysts

	Integral areas				
Catalysts	Peak 1 (164–181 °C)	Peak 2 (218–258 °C)	Peak 3 (315–390 °C)	Peak 4 (511–620 °C)	Total NO_x desorption (mmol g^{-1})
CeWTi	1919	3141	2121	1461	2.05
CeTi	1524	2668	2016	1336	1.87
CeWSiTi	786	1531	1991	751	1.29
CeSiTi	540	914	1162	1064	1.02

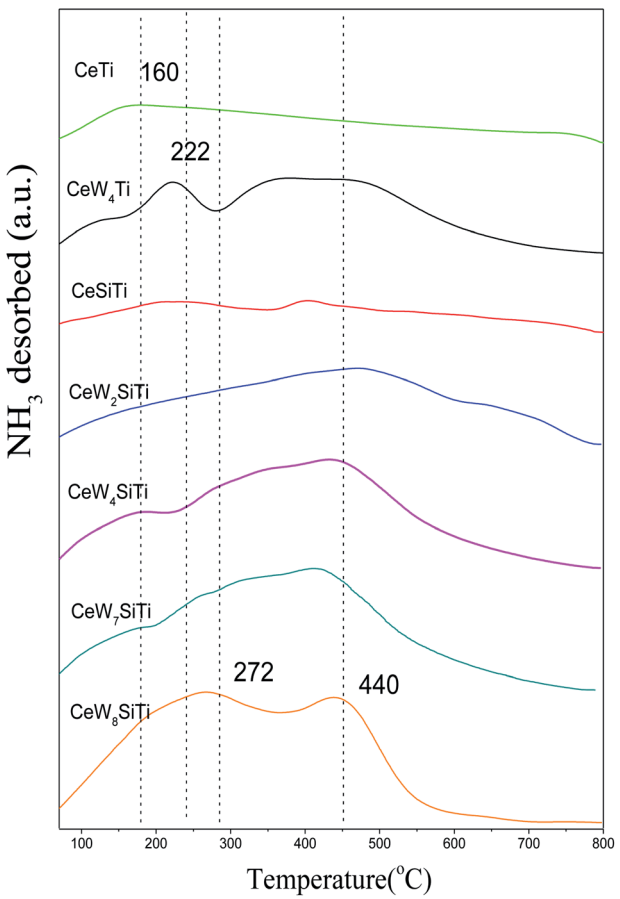

Fig. 7 NH_3–TPD profiles of CeW_xSi_yTi catalysts.

Table 5 Calculated amount of ammonia desorption in NH_3–TPD tests and hydrogen consumption in the H_2-TPR

Catalysts	NH_3 desorption (mmol g^{-1})	H_2 consumption (mmol g^{-1})
CeSiTi	0.14	1.47
CeW_2SiTi	0.38	5.44
CeW_4SiTi	1.38	6.68
CeW_7SiTi	1.50	8.17
CeW_8SiTi	2.02	8.65
CeTi	0.61	4.41
CeW_4Ti	1.01	4.70

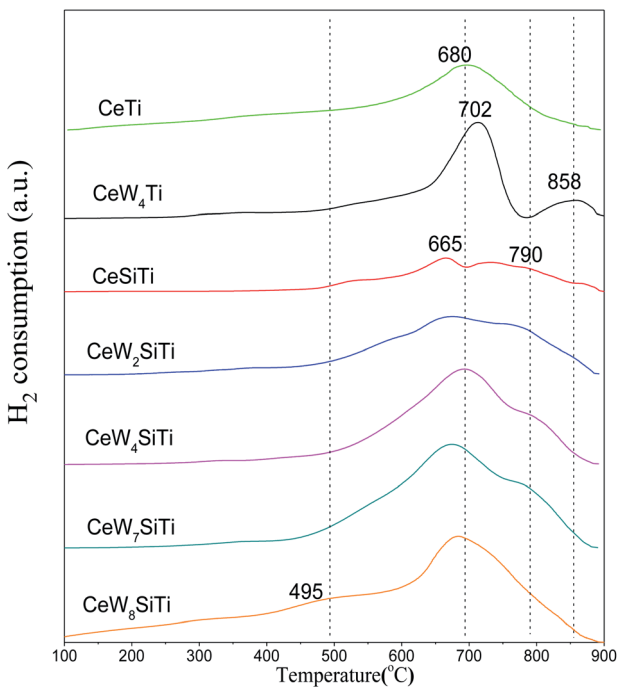

Fig. 8 H_2-TPR profiles of CeW_xSi_yTi catalysts.

reduction of bulk oxygen in ceria. For CeWTi and CeW_xTiSi catalysts, it is observed that reduction peaks of CeO_2 and WO_3 overlapped on the catalysts in the temperature range of WO_3 reduction. The broad overlapping peaks ranged from 665 to 702 °C are attributed to the reduction of WO_3 to WO_2 as well as bulk oxygen of CeO_2,[2,27] which is due to the interaction of tungsten with cerium oxide. The reduction peaks ranged from 790–858 °C were ascribed to the reduction of WO_2 to W.[29] The second reduction peak of the WO_x-containing catalysts shifted to higher temperatures, revealing a strong interaction between CeO_2 and WO_3 species with WO_3 addition. For CeW_xTiSi catalysts, with WO_3 content increasing, H_2 consumption increased from 1.47 mmol g^{-1} to 8.65 mmol g^{-1} as shown in Table 5, indicating that the addition of WO_3 could bring more reducible subsurface oxygen and increase the redox property, which facilitates SCR reaction. The results are in accordance with SCR activities.

4. Conclusion

In this work, WO_3 was doped into CeO_2/TiO_2 and CeO_2/TiO_2–SiO_2 catalysts by impregnation method. WO_3 has a promotional effect

on the activity of the catalysts and the optimal loading of WO_3 species was 7%. After hydrothermal aging treatment, NO_x conversion of W-containing catalysts at 500–600 °C even exceeded that of fresh samples, showing excellent hydrothermal stability. XRD and BET results show that the addition of WO_3 could promote CeO_2 and WO_3 crystallites disperse better over the catalyst surface. XPS results prove that WO_3 bring more appearance of Ce^{3+} and surface chemisorbed oxygen species so that more NO would be oxidized to NO_2, which was a benefit for the SCR process. NH_3 and NO_x–TPD results indicate that WO_3 provide more acid sites and more adsorbed NO_x and NH_3 species, which was also beneficial for the SCR reaction. TPR results suggest that WO_3 improve redox property of the catalysts.

Introduction of SiO_2 lower the catalytic activities of the catalysts. While after hydrothermally treating, the surface area of SiO_2-containing catalysts mostly preserved, hence enhancing the hydrothermal stability of the catalysts. There is synergistic effect between SiO_2 and WO_3 on keeping hydrothermal stability of the catalysts. From the results of XPS, TPD and H_2-TPR, the strong interaction between ceria, tungsten and silica could contribute to the excellent deNO_x performance of CeW_xTiSi_y mixed oxide catalyst.

Conflicts of interest

There are no conflicts to declare.

Acknowledgements

This research was funded by the Science and Technology Projects of China Northern Rare Earth (Group) High-tech Co., Ltd. (Grant No. BFXT-2018-D-1) and Natural Science Foundation of Inner Mongolia (Grant No. 2017MS0209).

References

1 J. Chen, Y. Chen, M. Zhou, Z. Huang, J. Gao, Z. Ma, J. Chen and X. Tang, *Environ. Sci. Technol.*, 2017, **51**, 473–478.
2 Y. Jiang, Z. Xing, X. Wang, S. Huang, X. Wang and Q. Liu, *Fuel*, 2015, **151**, 124–129.
3 S. Liu, X. Feng, J. Liu, Q. Lin, L. Xiong, Y. Wang, H. Xu, J. Wang and Y. Chen, *New J. Chem.*, 2019, **43**, 2258–2268.
4 F. Liu, Y. Yu and H. He, *Chem. Commun.*, 2014, **50**, 8445–8463.
5 J. Wang, H. Zhao, G. Haller and Y. Li, *Appl. Catal., B*, 2017, **202**, 346–354.
6 H. Hu, S. Cai, H. Li, L. Huang, L. Shi and D. Zhang, *J. Phys. Chem. C*, 2015, **119**, 22924–22933.
7 D. W. Kwon and S. C. Hong, *Appl. Surf. Sci.*, 2015, **356**, 181–190.
8 W. Zhao, Y. Tang, Y. Wan, L. Li, S. Yao, X. Li, J. Gu, Y. Li and J. Shi, *J. Hazard. Mater.*, 2014, **278**, 350–359.
9 W. Shan, F. Liu, Y. Yu and H. He, *Chin. J. Catal.*, 2014, **35**, 1251–1259.
10 J. Xu, H. Yu, C. Zhang, F. Guo and J. Xie, *New J. Chem.*, 2019, **43**, 3996–4007.
11 L. Chen, J. Li and M. Ge, *J. Phys. Chem. C*, 2009, **113**, 21177–21184.
12 Z. Yan, X. Shi, Y. Yu and H. He, *J. Environ. Sci.*, 2018, **73**, 155–161.
13 G. Zhang, W. Han, H. Zhao, L. Zong and Z. Tang, *Appl. Catal., B*, 2018, **226**, 117–126.
14 T. Boningari, A. Somogyvari and P. G. Smirniotis, *Ind. Eng. Chem. Res.*, 2017, **56**, 5483–5494.
15 L. Xu, C. Wang, H. Chang, Q. Wu, T. Zhang and J. Li, *Environ. Sci. Technol.*, 2018, **52**, 7064–7071.
16 Y. Geng, H. Huang, X. Chen, H. Ding, S. Yang, F. Liu and W. Shan, *RSC Adv.*, 2016, **6**, 64803–64810.
17 X. Gao, Y. Jiang, Y. Fu, Y. Zhong, Z. Luo and K. Cen, *Catal. Commun.*, 2010, **11**, 465–469.
18 Y. Peng, C. Liu, X. Zhang and J. Li, *Appl. Catal., B*, 2013, **140**, 276–282.
19 W. Shan, F. Liu, H. He, X. Shi and C. Zhang, *Chem. Commun.*, 2011, **47**, 8046–8048.
20 W. Zhao, Z. Li, Y. Wang, R. Fan, C. Zhang, Y. Wang, X. Guo, R. Wang and S. Zhang, *Catalysts*, 2018, **8**, 375.
21 L. Kang, H. Liu, H. He and C. Yang, *Fuel*, 2018, **234**, 1229–1237.
22 Q. Luo, Q. Zhou, Y. Lin, S. Wu, H. Liu, D. Cheng, Y. Zhong and C. Yang, *Catal. Sci. Technol.*, 2019, **9**, 6166–6179.
23 S. Wu, Y. Lin, C. Yang, C. Du, Q. Teng, Y. Ma, D. Zhang, L. Nie and Y. Zhong, *Chemosphere*, 2019, **237**, 124478.
24 L. Qiu, Y. Cheng, C. Yang, G. Zeng, Z. Long, S. Wei, K. Zhao and L. Luo, *RSC Adv.*, 2016, **6**, 17036.
25 L. Zong, J. Zhang, G. Lu and Z. Tang, *Catal. Surv. Asia*, 2018, **22**, 105–117.
26 L. Chen, J. Li, M. Ge and R. Zhu, *Catal. Today*, 2010, **153**, 77–83.
27 W. Shan, Y. Geng, X. Chen, N. Huang, F. Liu and S. Yang, *Catal. Sci. Technol.*, 2016, **6**, 1195–1200.
28 W. Shan, F. Liu, H. He, X. Shi and C. Zhang, *Appl. Catal., B*, 2012, **115**, 100–106.
29 L. Cao, X. Wu, Y. Xu, Q. Lin, J. Hu, Y. Chen, R. Ran and D. Weng, *Catal. Commun.*, 2019, **120**, 55–58.
30 L. Qiu, Y. Wang, D. Pang, F. Ouyang and C. Zhang, *Catal. Commun.*, 2016, **78**, 22–25.
31 M. Kobayashi, R. Kuma and A. Morita, *Catal. Lett.*, 2006, **112**, 37–44.
32 K. K. Akurati, A. Vital, J. P. Dellemann, K. Michalow, T. Graule, D. Ferri and A. Baiker, *Appl. Catal., B*, 2008, **79**, 53–62.
33 Y. Peng, K. Li and J. Li, *Appl. Catal., B*, 2013, **140**, 483–492.
34 Z. Ma, D. Weng, X. Wu and Z. Si, *J. Environ. Sci.*, 2012, **24**, 1305–1316.
35 Y. Wang, Z. Li, R. Fan, X. Guo, C. Zhang, Z. Ding, R. Wang and W. Liu, *Catalysts*, 2019, **9**, 797.
36 L. Chen, D. Weng, J. Wang, D. Weng and L. Cao, *Chin. J. Catal.*, 2018, **39**, 1804–1813.
37 Z. Wu, R. Jin, Y. Liu and H. Wang, *Catal. Commun.*, 2008, **9**, 2217–2220.
38 F. Liu and H. He, *J. Phys. Chem. C*, 2010, **114**, 16929–16936.
39 J. Li, Y. Zhu, R. Ke and J. Hao, *Appl. Catal., B*, 2008, **80**, 202–213.
40 J. Li, J. Hao, L. Fu, T. Zhu, Z. Liu and X. Cui, *Appl. Catal., A*, 2004, **265**, 43–52.

